Volume 5 | Number 9 | 7 March 2017 | Pages 1691–1864

Journal of Materials Chemistry B

Materials for biology and medicine

rsc.li/materials-b

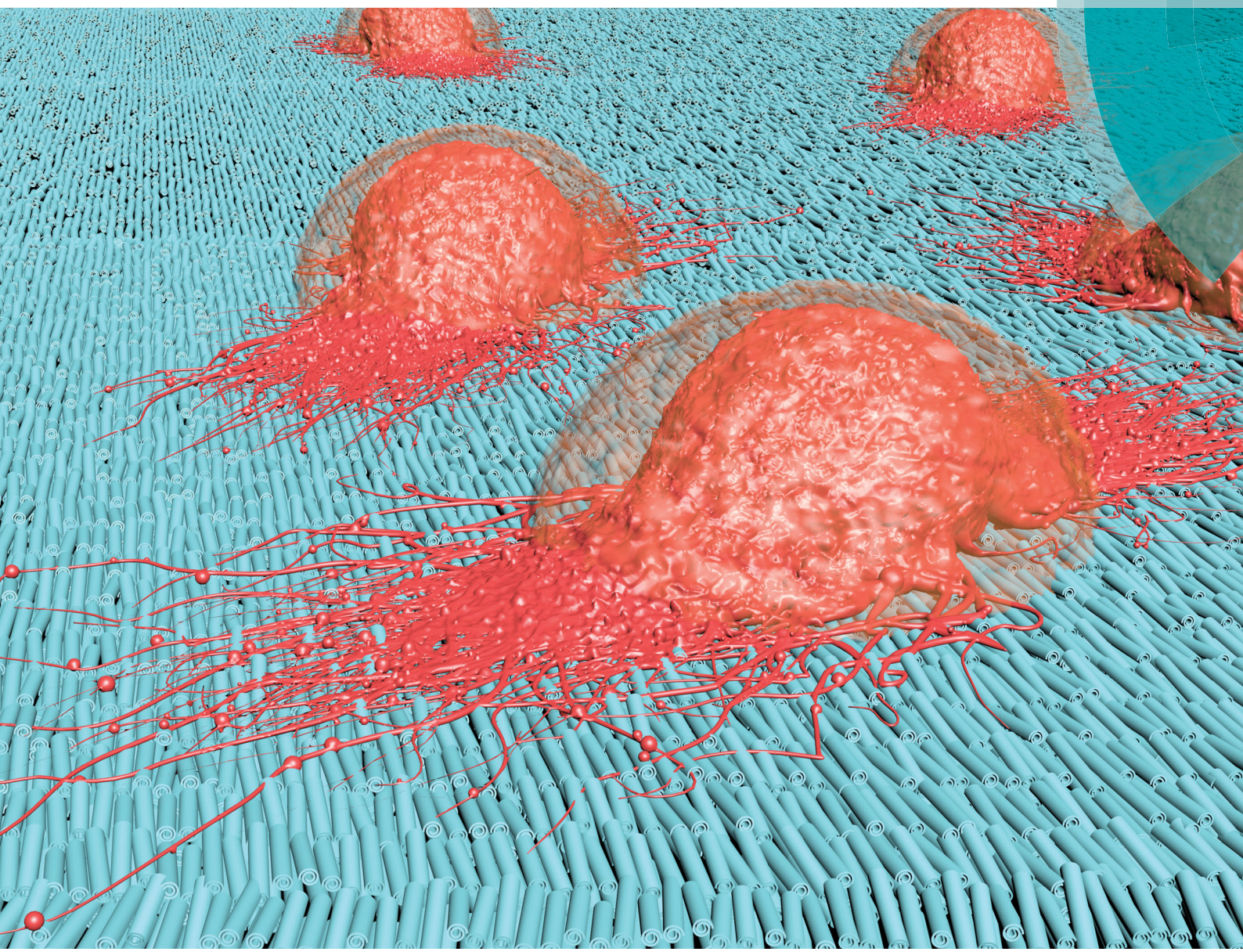

ISSN 2050-750X

ROYAL SOCIETY OF CHEMISTRY

PAPER

Mingxian Liu, Changren Zhou *et al.*

Large-area assembly of halloysite nanotubes for enhancing the capture of tumor cells

Journal of Materials Chemistry B

Materials for biology and medicine

rsc.li/materials-b

The Royal Society of Chemistry is the world's leading chemistry community. Through our high impact journals and publications we connect the world with the chemical sciences and invest the profits back into the chemistry community.

IN THIS ISSUE

ISSN 2050–750X CODEN JMCBDV 5(9) 1691–1864 (2017)

Cover
See Mingxian Liu, Changren Zhou *et al.*, pp. 1712–1723.
Image reproduced by permission of Mingxian Liu from *J. Mater. Chem. B*, 2017, **5**, 1712.

REVIEW

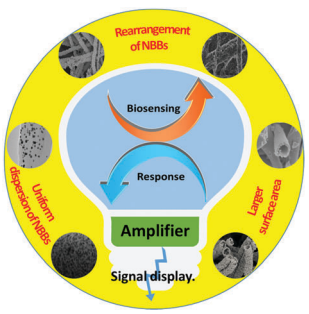

PAPERS

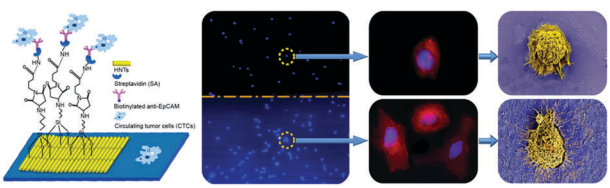

Journal of
Materials Chemistry B

PAPER

Cite this: J. Mater. Chem. B, 2017, 5, 1712

Large-area assembly of halloysite nanotubes for enhancing the capture of tumor cells†

Rui He, Mingxian Liu,* Yan Shen, Zheru Long and Changren Zhou*

Received 28th September 2016,
Accepted 16th January 2017

DOI: 10.1039/c6tb02538b

rsc.li/materials-b

Here, polystyrene sulfonate sodium (PSS) modified Halloysite nanotubes (HNTs) were self-assembled into a patterned coating on a glass substrate with ordered nanotube arrays in a slit-like confined space. The microstructure of the formed patterned HNTs coating was investigated. The formed strips are more regular and almost parallel to each other with an increase in HNTs concentration. The HNTs coating formed from the 2% PSS-HNTs dispersion has the maximum nanotube alignment degree. The patterned HNTs coating was employed to capture tumor cells. The tumor cells can be captured by the HNTs coating effectively compared with a smooth glass surface due to the enhanced topographic interactions between the HNTs coating and cancer cells. The HNTs coating prepared from the 2% PSS-HNTs dispersion has the highest capture yield which is due to the ordered nanotube arrangement and the appropriate surface roughness. The HNTs coating was further conjugated with anti-EpCAM, which leads to the capture yield of MCF-7 cells reaching 92% within 3 h. The HNTs coating can capture 8 MCF-7 cells from 1 mL artificial blood samples spiked with 10 MCF-7 cells, showing the promising applications of HNTs in clinical circulating tumor cell capture for early diagnosis and monitoring of cancer patients.

1. Introduction

Circulating tumor cells (CTCs) are cells that have shed into the vasculature from a primary tumor and they can be carried around the body. Because the number of CTCs in circulating blood is extremely low (about a few to hundreds of CTCs per milliliter of blood), the efficiency of CTC separation is not satisfactory. The common methods suffer many disadvantages such as low capture specificity, easy to cause cell damage, and high operating costs, which affect the accuracy of the corresponding cancer diagnosis. The tumor cell surface has many nanostructures, such as filiform or flake pseudopodia, microvilli, and so on, which can interact with artificial nanostructures. The interactions significantly affect the cell adhesion, growth, differentiation, protein expression, and other life activities.[1] A lot of inorganic or organic materials with nanostructures, such as nanospheres,[2] nanotubes,[3] nanorods,[4] nanofibers,[5] and nanoplates,[6,7] have been used to design the CTC separation interface. Nanostructures conjugated with antibody can recognize and bind specifically to cancer cells.[8] Additionally, nanorough surfaces without antibodies can also capture CTCs due to the unique cell–material interactions.[9] Many types of nanoparticles were reported to achieve this goal, such as silicon nanowires,[10,11] silica nanospheres,[12] titanium dioxide nanofibers,[5] titanium dioxide nanospheres,[2] graphene oxide (GO) nanoplates,[6,7] and polymer nanostructures.[13–17] The reported CTC capture efficiency can be as high as 90% and capture sensitivity can reach several cancer cells per milliliter of blood. For example, Nagrath *et al.* developed a kind of chip based on GO nanofilms to sensitively capture cancer cells and the capture ability was four tumor cells from one milliliter of blood.[7] Although many nanomaterials have been developed to capture tumor cells, there still exist many flaws for their clinical application, such as the expensive price of synthetic nanomaterials, the difficulty of preparing the nanostructures, the poor reproducibility of the device, low capture yield, and the high cost of the graft antibody. It is very necessary to search abundant and reliable materials to further improve the CTC capture.

In recent years, halloysite nanotubes (HNTs) as new one-dimensional nanomaterials have become the focus of intensive research in biomedical areas,[18–21] which is owing to their distinctive nanotubular structure, good biocompatibility, high adsorption ability, low price, and various potential applications. HNTs are a 1 : 1 aluminosilicate clay mineral with the empirical formula $Al_2Si_2O_5(OH)_4$. HNTs have a diameter of 30–70 nm and a length of 200–1500 nm, which gives a high aspect ratio of 2.8–50. Firstly, modified HNTs and their polymer composites can be used as nanocarriers for different drugs including chemical drugs, traditional Chinese medicine, and biological medicine.[19,22,23] HNTs can prolong the half-life of drugs, increase the loading amount of drugs, and improve the sustained release performance of drugs. For example, the curcumin loaded chitosan grafted HNTs showed

Department of Materials Science and Engineering, Jinan University, Guangzhou 510632, China. E-mail: liumx@jnu.edu.cn, tcrz9@jnu.edu.cn; Fax: +86-20-85223271

† Electronic supplementary information (ESI) available. See DOI: 10.1039/c6tb02538b

specific toxicity to various cancer cell lines, including HepG2, MCF-7, SV-HUC-1, EJ, Caski and HeLa, and demonstrate an inhibition concentration of IC_{50} at 5.3–192 μM.[24] As nanoparticles with high aspect ratios, HNTs have also been incorporated into biodegradable polymers to reinforce their mechanical properties for application as tissue engineering scaffolds.[25–27] The compressive strength and modulus of these composite scaffolds are significantly enhanced without the sacrifice of biocompatibility. Thirdly, HNTs can be labeled *via* grafting of fluorescein and radioactive elements, which can be used to fabricate biosensors for disease diagnosis and study the pathogenesis. Fluorescein isothiocyanate isomer I (FITC) labeled HNTs could be taken up by tumor cells and located in the nuclear vicinity within the cells.[28] The *in vivo* distribution of Rhodamine B labeled HNTs was also investigated using *P. caudatum* and the results showed that HNTs were not cytostatic at low concentrations (1 mg mL^{-1}).[29] Lastly, using HNTs as CTCs the capture device has been studied since the year 2010.[3,30–34] High efficacy capture of cancer cells was realized by coating the modified HNTs on plastic microtubes with or without the antibodies.[31,33] The enhanced cell capture property is attributed to the altered nanoscale topography by the nanosized HNTs. HNTs coating was found to increase the surface area onto which molecules could adsorb, as well as present molecules into the hydrodynamic lubrication layer that slowed the sedimentation of cells to the device surface.[33] Although the HNTs coated microrenathane tubes exhibited a significant increase in cancer cell adhesion while simultaneously repelling leukocyte adhesion, the preparation process of the device was complicated and the capture cells are hard to stain and count. Our recent study also found that the rough nanosurfaces formed by drying HNTs on capillary tubes can also be used to capture cancer cells.[35]

In the present work, we prepare patterned HNTs coatings on a flat glass substrate *via* drying the HNTs aqueous dispersion in a slit-like confined space. To increase the stability of HNTs in water, polystyrene sulfonate sodium (PSS) was firstly adsorbed on the surface of the nanotubes. Then the PSS-HNTs dispersion was injected into the slit composed of two glass slides and subsequently dried at 60 °C. Patterned HNTs coatings with ordered nanotube arrays and regular cracks were then formed. The microstructure of the surfaces was dependent on the concentration of the dispersion. A variety of tumor cells, including MCF-7, HepG2, Neuro-2a, A549, and B16F10, were used to investigate the capture efficacy of the HNTs coating. The capture efficacy is related to the surface roughness of the HNTs coating. To further increase the capture efficacy of the HNTs coating, anti-EpCAM was conjugated on the surface of HNTs. The antibody conjugated HNTs surface showed 92% capture efficacy towards MCF-7 at 3 h. All these results suggest that the patterned HNTs coatings show promising applications in cancer diagnosis.

2. Materials and methods

2.1 Materials

Halloysite nanotubes (HNTs) were purchased from Guangzhou Runwo Materials Technology Co., Ltd, China. The elemental composition of HNTs by X-ray fluorescence (XRF) was determined as follows (wt%): SiO_2, 54.29; Al_2O_3, 44.51; Fe_2O_3, 0.63; TiO_2, 0.006. Polystyrene sulfonate sodium salt (PSS, MW 70 000), streptavidin (SA), and biotinylated anti-human-EpCAM/TROP1 antibody (goat IgG) were purchased from Sigma-Aldrich. Diamidino-2-phenylindole dihydrochloride (DAPI), rhodamine phalloidin, phosphate-buffered saline (PBS), Triton X-100, and 0.25% Trypsin-EDTA (Gibco, 1×) were purchased from Jiangsu KeyGEN BioTECH Co., Ltd, China. Butanedioic anhydride, 3-aminopropyltriethoxy silane (APTES), *N*,*N*-dimethyl formamide (DMF), *N*-hydroxysuccinimide (NHS), and 1-ethyl-3-(3-dimethylaminopropyl) carbodiimide hydrochloride (EDC) were purchased from Aladdin Industrial Corporation. Ultrapure water was prepared using a Milli-Q water system. Other chemicals were purchased from Aladdin and used without further purification.

2.2 Preparation of PSS modified HNTs

The PSS solution was prepared by dissolving PSS at the concentration of 2% (w/v) to modify the surface of HNTs according to the method of ref. 36. Then 2 g of raw HNTs was added to 100 mL of 2% PSS solution under continuous stirring for 2 days at 25 °C. The stirring was then stopped and the dispersion was allowed to stand for 1 h. The supernatant was then collected and centrifuged at 4000 rpm for 10 min. The product was washed 3 times with deionized water. The deposit at the bottom of the centrifuge tubes was dried under vacuum at 60 °C for 24 h and crushed into powder. The adsorbed PSS on HNTs was about 2.5% by thermogravimetric (TG) analysis. The modified HNTs samples were denoted as PSS-HNTs. The water contact angles of glass slides before and after modification were measured with KRUSS drop shape analyzer DSA 100 instrument at 25.0 ± 0.1 °C. The contact angle was measured just after the liquid deposition onto the substrate. The liquid droplet volume was 5.0 ± 0.5 μL.

2.3 Preparation of the patterned HNTs coating in a confined space

The patterned HNTs coating was prepared in a home-made device with a slit-like confined space composed of two glass slides and two gaskets (Fig. S1, ESI†). Glass slides were firstly washed with acetone and ethanol, and then were soaked in the Piranha solution (70% H_2SO_4, 30% H_2O_2) at 90 °C for 1 h, followed by washing with deionized water to bring them to neutral pH and dried by using nitrogen gas flow. About 1.5 mL of different concentrations of the HNTs dispersion was injected into a slit-like confined space. The confined space was composed of two glass slides (length × width: 7.5 × 2.5 cm) and two glass gaskets (the length × width × thickness: 1.5 × 2.5 × 0.2 cm). The middle and the side were sealed by adhesive tape and clamp respectively. The drying of the HNTs aqueous dispersion in the device was performed at 60 °C, and about 12 h was needed for complete drying of the dispersion. Finally, a series of patterned HNTs coatings with size of 4.5 × 2.5 cm (length × width) were obtained. To stabilize HNTs coating during cell culture and increase the electrostatic attractions between HNTs and cells, the HNTs coatings were soaked in 20 mL of 4% (v/v) APTES in anhydrous ethanol solution for 1 h. The excess APTES was

removed by washing the coating with anhydrous ethanol. A 1 × 1 cm patterned HNTs coating on a glass slide for cell capture was obtained by cutting the glass slide using a glazing knife. The blank glass slides without the HNTs coating was used as a control.

2.4 Characterization of patterned HNTs coatings

The morphology and the liquid crystal phenomenon of patterned HNTs coatings were observed using a stereoscopic microscope (ZEISS Stereo Discovery. V20, Germany) configured with a polarized light component. The microstructure of the coating was further analyzed using a field emission scanning electron microscope (SEM, Philips LEO1530 VPSEM) at 5 kV. The surface roughness of the HNTs coatings was characterized using an atomic force microscope (AFM) equipped with a NanoScope IIIa controller (Veeco Instruments Inc.). The quantitative analysis of root-mean-square roughness (R_q) and average roughness (R_a) was also acquired using the NanoScope Analysis Software.

2.5 Cell culture

Human breast cancer (MCF-7) cells, human hepatoma cells (HepG2), mouse neuroblastoma cells (Neuro-2A), human lung carcinoma cells (A549), metastatic murine melanoma cells (B16F10), mouse osteoblastic cells (MC3T3-E1), and human liver cells (L02) were purchased from the Laboratory Animal Center of Sun Yat-sen University. All the cells were maintained in DMEM (Life Technologies) supplemented with 10% bovine calf serum (FBS, Life Technologies) and 1% penicillin (100 U mL^{-1})/streptomycin (100 μg mL^{-1}). All cell lines were maintained at 37 °C in a humidified atmosphere of 5% CO_2 in air as a monolayer culture in plastic culture plates (25 cm^2, Corning, NY, 14831). The cells were grown to ~80% confluence before passaging with trypsin/ethylenediaminetetraacetic acid (EDTA) (Life Technologies) incubation for 2–3 min.

2.6 Cell capture and characterization

The APTES treated HNTs coatings on glass slides were sterilized by microwave radiation in a commercial microwave oven at 700 W (2450 MHz) for 2 min. Then the patterned HNTs coatings (1 × 1 cm) were placed in 24-well cell culture plates and then 1 mL of the cell suspension (1 × 10^4 cells mL^{-1}) was added into each well. After standing for 1 h, 2 h, and 3 h in a cell incubator (37 °C, 5% CO_2, HF 100, Heal Force Bio-Miditech Ltd, China), the substrate with HNTs coating was rinsed with PBS 3 times. The captured cells were fixed with paraformaldehyde solution (4 wt% in PBS) for 10 min and penetrated with Triton-X100 (0.2 wt% in PBS) for 10 min. The cells were dyed with DAPI solution (5 μg mL^{-1} in PBS) for 5 min and washed with PBS 3 times to remove excess DAPI. Imaging and counting of the cells captured by the HNTs coatings were performed with fluorescence microscopy images recorded using a fluorescence microscope (EVOS® FL Cell Imaging System) and ImageJ software (National Institutes of Health, USA) respectively. At least 10 images of the captured cells were recorded at 50× magnification. The capture efficiency was calculated by comparing the captured cell number with the initial number of cells added to the well (1 × 10^4 cells). To investigate the interactions between tumor cells and HNTs coatings, the captured cells were dyed firstly by adding 300 μL of rhodamine phalloidin (80 nM) and then 300 μL of DAPI (10 μg mL^{-1} concentration) in each well. The morphology of captured cells in the HNTs coatings was further analyzed by SEM and AFM. Before SEM observation, the cells were then fixed with 2.5% glutaraldehyde in cacodylate buffer (Karnovsky fixation solution) at 4 °C for 24 h and then dehydrated in ethanol at 30, 50, 70, 80, 90, 95 and 100% concentration. The samples were then freeze-dried at −80 °C. AFM analysis of the cells was performed in contact mode. The curvature radius of the silicon tip is less than 10 nm, the force constant is 0.6 N m^{-1}, and the scan rate is 0.3 to 1 Hz. The acquired images (50 × 50 μm) were processed using the instrument-equipped software (NanoScope Analysis Software) to eliminate low-frequency background noise (flatten order: 0 to 2) in the scanning direction.

2.7 Bioconjugation with anti-EpCAM on the HNTs coatings

The APTES treated HNTs coatings were soaked with 20 mL of 2% (w/v) butanedioic anhydride in DMF solution at room temperature for 1 day. The substrate was rinsed 3 times with deionized water to remove the unbounded butanedioic anhydride. Then the coating was treated with 2% (w/v) NHS solution in deionized water for 30 min and then 1% (w/v) EDC solution for 2 h. Next, 10 μg mL^{-1} SA solution in PBS was added to the HNTs coating and kept at 4 °C overnight. Afterwards, the coatings were washed 3 times with PBS and conjugated with anti-EpCAM (10 μg mL^{-1} in PBS) at room temperature for 2 h. The capture process of cells was similar to the previous procedure.

2.8 Capture of tumor cells in peripheral blood samples

The blood samples were obtained from healthy donors and preserved in blood collection tubes before use (containing EDTA). The number of the MCF-7 cells was measured with a hemocytometer several times to multiple configuration 1 × 10^3 cells per mL of the cell suspension. Then the cell suspension was diluted to different numbers of MCF-7 cells (10, 20, 50, 100 and 200 per milliliter). Different numbers of MCF-7 cells were spiked artificially into 1 mL of the blood sample (diluted by the same volume of DMEM) or DMEM. The solution samples with tumor cells were then added onto the anti-EpCAM conjugated HNTs coating. After static capturing for 2 h and then rinsed with PBS, the cells were fixed and penetrated for 10 min. Subsequently, the tumor cells were identified and counted from non-specifically captured white blood cells (WBCs) using a commonly used three-color immunocytochemistry method,[37] including PE-labeled anti-Cytokeratin 19 (CK19, a protein marker for epithelial cells), FITC-labeled leukocyte common antigen (anti-CD45, a marker for white blood cells) and DAPI for nuclear staining. These cells were imaged by using an inverted XDY-2 microscope (Guangzhou Yuexian optical instrument Co., Ltd, China).

3. Results and discussion

3.1 Patterned HNTs coating formed in a confined space

PSS is a macromolecular surfactant which can be ionized into positively charged Na^+ ions and negatively charged polystyrene

sulfonic groups in water. The negatively charged polystyrene sulfonic groups can be adsorbed on HNTs at an internal surface, which leads to an increase of the zeta potential value of HNTs in the aqueous solution. PSS can increase the dispersion of HNTs in aqueous dispersion.[36,38] The increased dispersibility of HNTs in water is critical for their self-assembly and the formation of patterned coatings in the following step. The glass slide surfaces are treated by Piranha solution to produce a large number of hydroxyl groups, which is of benefit for the formation of hydrogen bonds between HNTs and the glass substrate. The strong interfacial interactions lead to robust HNTs coatings on the glass surfaces (Fig. S1, ESI†). The water contact angle of the glass slides before and after surface treatment was measured (Fig. S2, ESI†). The contact angle of the treated glass slide (7.1°) is smaller than that of control (35.4°). This suggests that a large number of hydroxyl groups is present on the treated glass slide surface.[39] As shown in Fig. 1, about 1.5 mL of PSS-HNTs aqueous dispersion was injected into the confined space prepared by two glass slides and two gaskets. After drying at 60 °C for 12 h, water is exhausted by evaporation and HNTs assemble in the confined space due to the surface tensions. This process results in a uniform coating with some strips or cracks on the surface of the glass slide. The appearance of the formed HNTs coating on glass slides is shown in Fig. 2(A). The coating formed at a relatively low HNTs concentration (1%) is totally transparent. Upon increasing the concentration of the HNTs dispersion, the transparency of the coating is getting worse. However, all the coating is semitransparent and therefore it is convenient for observing the captured cells by DAPI staining. The HNTs coatings exhibit a rough surface which can be used to capture tumor cells.

To further characterize the formed HNTs coatings, stereoscopic microscopy images were taken with different magnifications (Fig. 2(B)). It is clear that the higher the concentration of the PSS-HNTs dispersion is, the wider the strips formed on the glass slide surface are. There is almost no strip formed but several tiny fragmentations on the stripes formed when drying the PSS-HNTs dispersion with a concentration below 1%. When the PSS-HNTs concentration increases, the formed strips are more regular and almost parallel to each other. When the concentration of the PSS-HNTs dispersion reaches 10%, the strips have a certain radian at the edges. The formed strip width (W) is in the range of 50–120 μm, which depends on the concentration of HNTs dispersion. The formation of patterned surfaces is a consequence of controlled, repetitive stick–slip motion of the contact line of the dispersion that resulted from the force balance between pinning force (surface tension) and depinning force (gravity) during the irreversible solvent evaporation.[40,41] The HNTs strips propagate from the top towards the bottom. As the water in the dispersion evaporated, HNTs remain on the surface of the glass slide and form a solid–liquid–gas three phase contact line. When the gravity is higher than the surface tension, the contact line will slip to another position. The stick process leads to the formation of strips and the slip process leads to the formation of crack between strips. When the concentration of the HNTs dispersion is low, the stick–slip motion is weak which results in relatively small strip width and strip space. Our previous study also showed that the strip width and space increases with the HNTs concentration.[35]

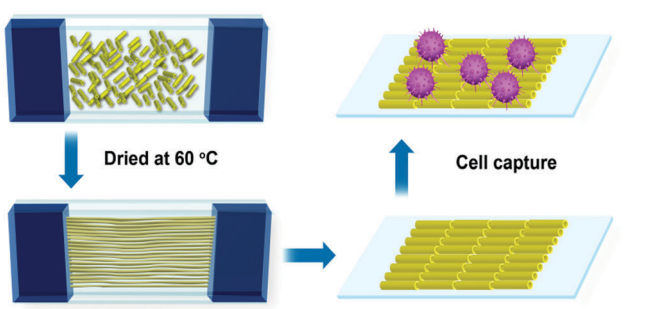

Fig. 1 Schematic illustration of the preparation and tumor cell capture process of patterned HNTs coating.

Interestingly, the patterned HNTs coatings exhibit a liquid crystal-like optical phenomenon. The polarized light microscopy (PLM) is a method to examine the arrangement of the HNTs. It can be seen that the patterned HNTs coating shows an obvious polarization effect to polarized light (Fig. 2(C)). When the strips are horizontal, the field of vision is dark (Fig. 2(C)-(a)). When one rotates the HNTs coating anticlockwise, the PLM image gets bright gradually. When the rotation angle is 45°, the image becomes totally bright (Fig. 2(C)-(b)). Afterwards, the images turn dark and become totally dark when the strips are vertical. The images turn bright again when the rotation angle is 135° and then turn dark. These results suggest that the patterned HNTs coating has a liquid crystal-like light property.[42] The liquid crystal phenomenon suggests a regular alignment of the nanotubes in the coating.

To illustrate the microstructure of the patterned HNTs coating, SEM was performed on the samples (Fig. 3(A)). The SEM photos of the coatings formed by drying different concentrations of the PSS-HNTs dispersion are in accordance with the optical microcopy result above. All the HNTs coatings on the glass substrate are homogenous with uniform thickness. Stripe-like HNTs patterns with a regular distance between adjacent strips were prepared by controlled evaporative self-assembly of the PSS-HNTs solution in a confined geometry consisting of two glass slides and two gaskets. During the hot drying, as water evaporated fast from the top of the solution, the nanotubes were transported to the drying line of the confined solution to pin the three-phase contact line (*i.e.*, "stick"). As the deposition process progressed, the initial contact angle of the meniscus at the edge gradually decreased to a critical value because of continuous evaporative loss of water, at which the depinning force (*i.e.*, capillary force) became larger than the pinning force, causing the contact line to move toward the lower position (*i.e.*, "slip") and to stop at a new position, thereby leaving behind a local strip.[43] Such consecutive and controlled "stick–slip" cycles of the receding contact line in the slit-like confined geometry produced regular stripes in the substrate, which was a direct consequence of the competition between the linear depinning force and the nonlinear capillary force. The strip width increases with the HNTs

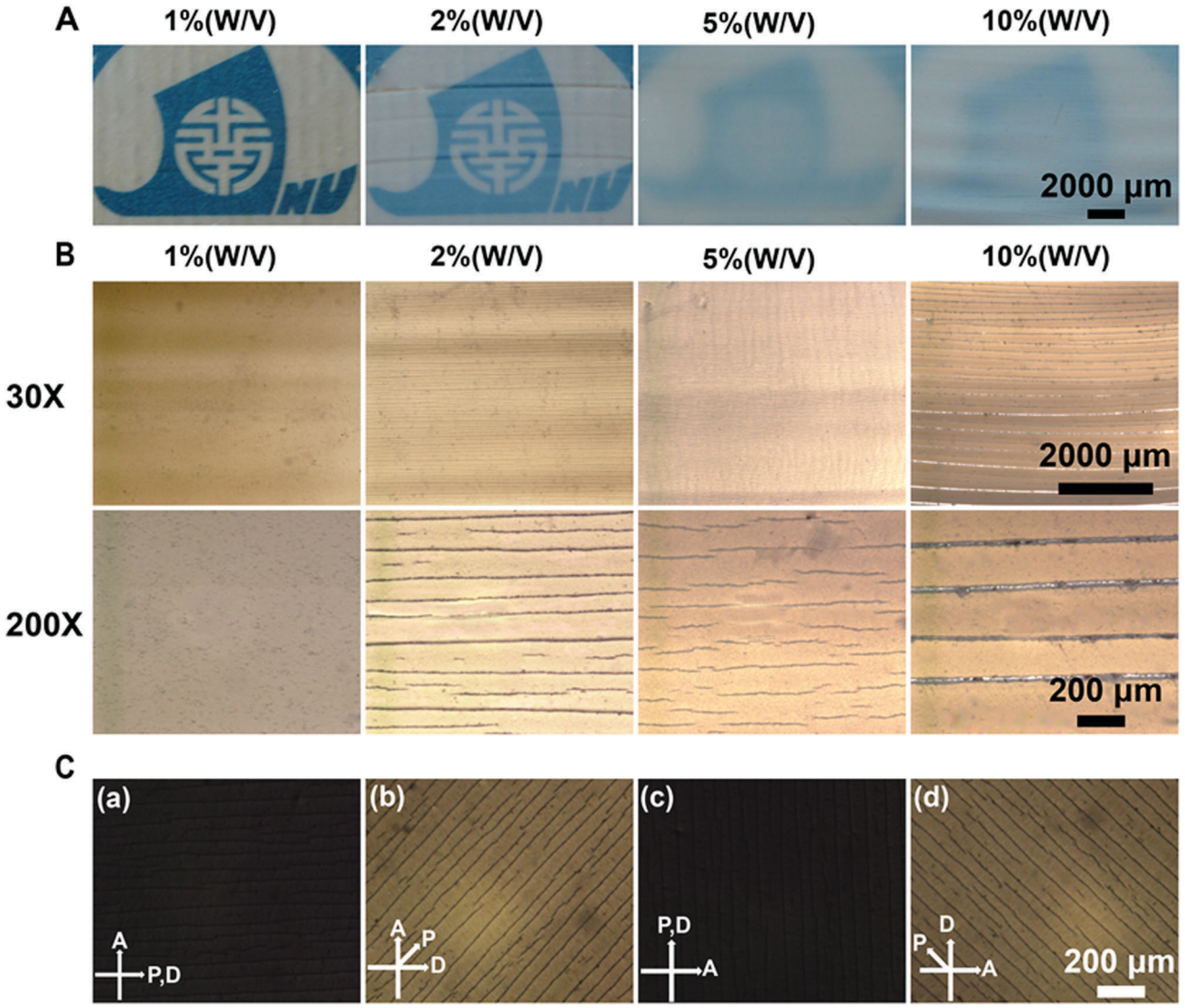

Fig. 2 The photograph of the HNTs coating formed on the glass substrates from different PSS-HNTs aqueous dispersions at 60 °C (A); the optical microscopy image of the patterned HNTs surface at different magnifications (B); polarized light microscopy (PLM) images of HNTs coating at the extinction location (a and c) and light interference location (b and d) (C).

dispersion concentration. From the high magnification images, a regular arrangement of the nanotubes is found especially for the coating formed from 2% PSS-HNTs dispersion. The alignment degree of the nanotubes is low at other HNTs concentrations. This is due to the fact that the self-assembly of nanotubes is driven by their interfacial interactions *i.e.* charge repulsion. When the dispersion concentration of PSS-HNTs is high, HNTs particles can aggregate, which affects the self-assembly process. When the dispersion concentration of PSS-HNTs is low, such as 1%, the distance between the nanotubes is larger and self-assembly drive force is weaker. Therefore, HNTs are hard to self-assemble in an ordered manner at relatively low and relatively high dispersion concentrations. In total, the HNTs coating formed from 2% PSS-HNTs dispersion has the maximum nanotube alignment degree, which may benefit for enhancing the cell capture efficacy.[35] The advantages of the prepared patterned HNTs coating over the coating prepared by the droplet-casting method lie in that this routine can obtain a homogenous HNTs coating with a large area.

Previous studies showed that the surface roughness of the substrate can significantly affect the interactions between materials and cells.[44,45] AFM was further applied to determine the influence of the concentration on the 3D morphology and surface roughness of HNTs coatings (Fig. 3(B)). The roughness increases with the concentration of the HNTs dispersion. For example, when the HNTs concentration is 1%, root-mean-square roughness (R_q) and average roughness (R_a) are 49 nm and 38.8 nm, whereas they are 94.4 nm and 74.5 nm for the 10% HNTs dispersion respectively. The surface roughness of the prepared HNTs coating is comparable with that of TiO_2 nanoparticle surfaces on a glass substrate for cancer cell capture (surface roughness from 36 to 94 nm).[2] Whereas in another study of cancer cell capture, the reduced GO nanosurfaces showed R_a from 40 nm to 20 μm which was obviously higher than that of

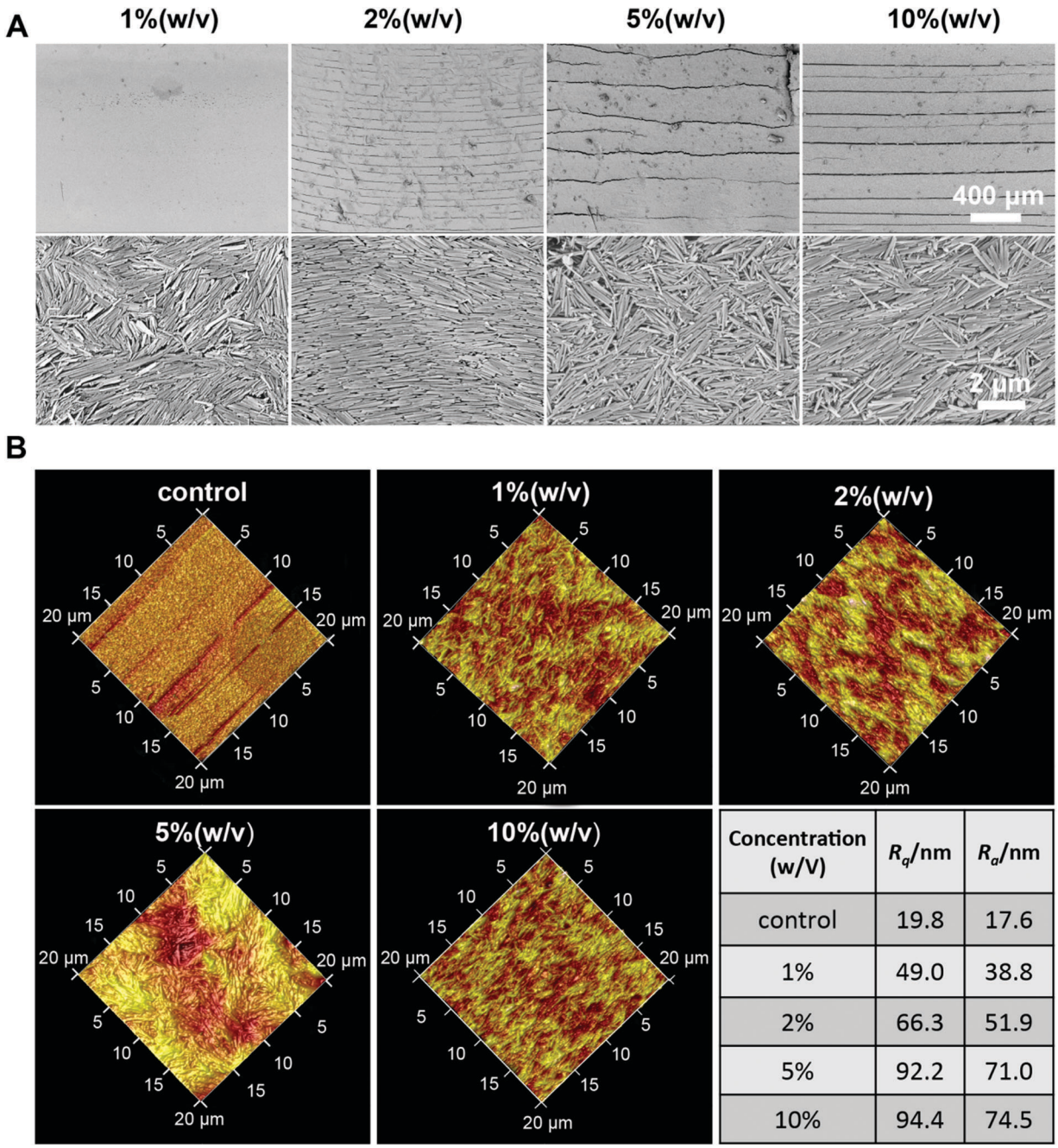

Concentration (w/V)	R_q/nm	R_a/nm
control	19.8	17.6
1%	49.0	38.8
2%	66.3	51.9
5%	92.2	71.0
10%	94.4	74.5

Fig. 3 SEM images (A) and AFM image and roughness statistical value of the patterned HNTs coating (B) formed from different PSS-HNTs dispersion concentrations.

the presently prepared HNTs coating.[6] Consistent with previous SEM results, the nanotube alignment is maximum in the patterned HNTs coating produced by drying 2% PSS-HNTs dispersion.

3.2 Capture of tumor cells by the patterned HNTs coating

Rough surface can influence diverse cell behaviors,[46,47] such as attachment, proliferation, and migration. HNTs can form patterned rough coatings on glass substrates *via* a simple evaporation induced self-assembly process. The patterned HNTs coating with proper roughness can be used to capture tumor cells. To investigate the effect of surface roughness of the substrate on the cell capture yields, the tumor cell capture experiment was performed on both the smooth glass surface and the rough HNTs coatings on the glass substrate. The roughness ranges from 19.8 nm to 94.4 nm for the samples. Fig. 4(A) shows the DAPI-staining fluorescence images of the captured L02 cell on a smooth glass slide and 2% (w/v) HNTs coatings for 1, 2 and 3 h. It can be seen that the L02 cell numbers on both substrates increase with the capture time. When compared with the two surfaces, it is clear that the rough HNTs surfaces can capture much more cells than those of smooth glass surfaces. The number of cells captured on the same areas of different surfaces was counted

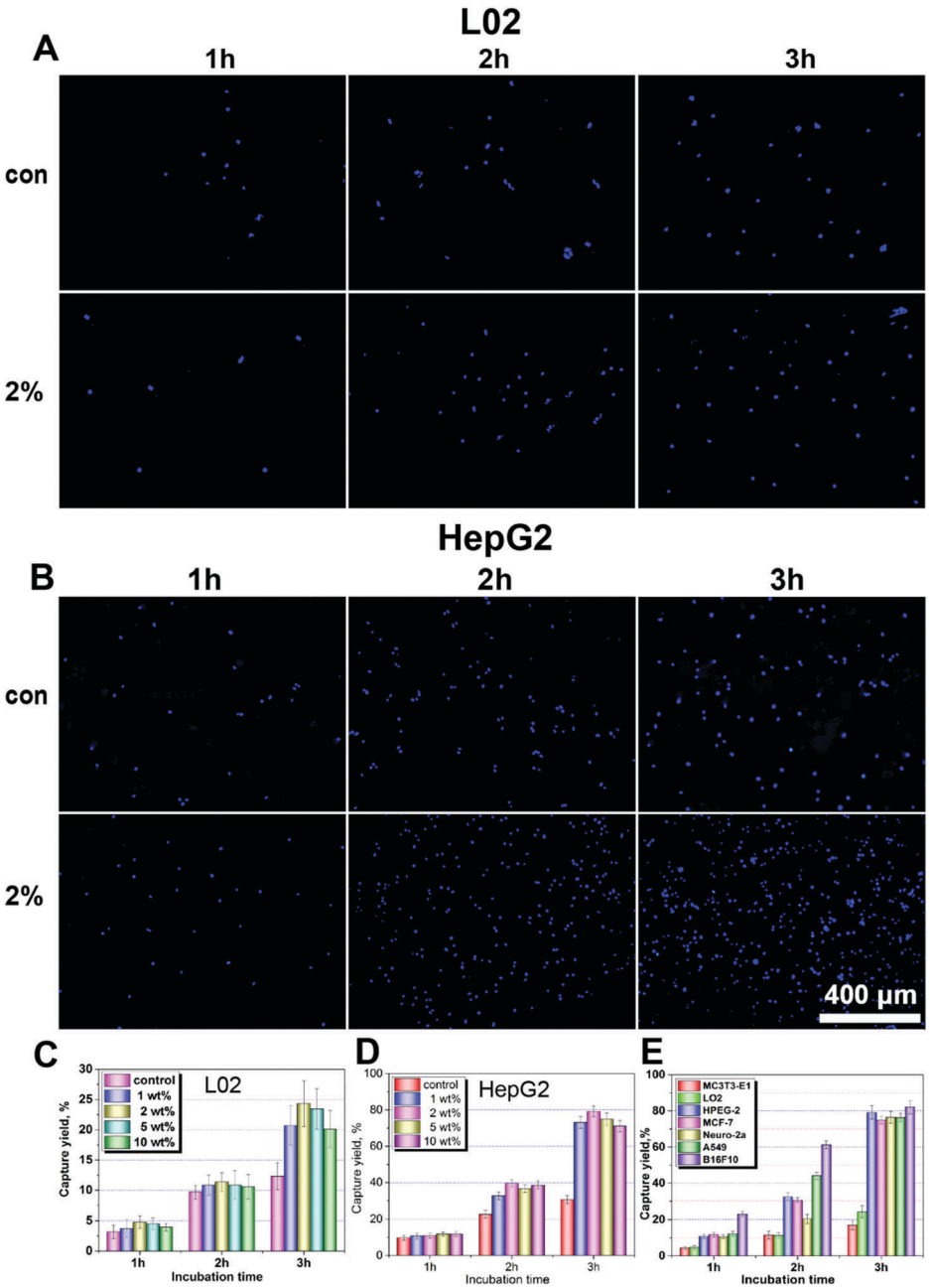

Fig. 4 The DAPI fluorescence microscopy images of captured cells of L02 (A) and HepG2 (B) on the blank glass and HNTs coating; L02 capture yield on the blank glass and different HNTs coatings with different incubation times (C); HepG2 capture yield on the blank glass and different HNTs coatings with different incubation times (D); capture yield of different cells on the HNTs coatings formed from 2% (w/v) PSS-HNTs concentration at different incubation times (E).

via ImageJ software to quantify the capture efficiency (Fig. 4(C)). Different HNTs rough surfaces show a cell capture yield of L02 cells in the range of 20–25% after 3 h incubation which is higher than the capture yield of the control group (12.5%). The 2% (w/v) HNTs coating has the highest capture yield compared to others, which may be attributed to the proper surface roughness of the coating. Compared with normal cells, tumor cells show a different structure such as possessing more pseudopods.[48] HepG2 cells were used to investigate the capture behavior of the tumor cells (Fig. 4(B)). Also, it can be found that after 1, 2, and 3 h of incubation, the captured cell number on the 2% (w/v) HNTs rough surfaces is much higher compared to the blank glass slide. Fig. 4(D) shows the relationship between HepG2 cell capture yield with incubation time for different HNTs coatings. With an increase in the cell incubation time, the capture yield increases significantly especially after 2 h. The HepG2 cell capture efficiencies on the HNTs rough surfaces are all higher than that on the blank glass surface after 1, 2, and 3 h of incubation. The 2% (w/v) HNTs rough surfaces have the highest cell capture yield of 79.2% for 3 h which is near 3-fold to the control group. A variety of tumor cells (MCF-7, HepG2, Nero-2a, A549 and B16F10) and normal cells (MC3T3-E1 and L02) were further used to

investigate the capture yield for the 2% HNTs coatings (Fig. 4(E)). It also can be seen that the patterned HNTs coatings show high capture yield for the tumor cells and show relatively low capture yield for the normal cell, which may due to the different surface structure of the cells. Among the used tumor cells, the capture yield of B16F10 by the HNTs rough surfaces without antibody conjugation is maximum and reaches 82.2% for 3 h capture.

Some studies indicated that the cells on the rough surface showed more flat morphology compared with those on the smooth surface.[49] The morphology of the captured tumor cells was investigated in detail. Fig. 5(A) shows the optical microscopy images of MCF-7 cells captured on a blank glass surface, 1% (w/v) HNTs rough surfaces, and 2% (w/v) HNTs rough surfaces for 3 h. Consistent with the previous result, the cell numbers on 2% (w/v) HNTs rough surfaces are much more than 1% (w/v) HNTs rough surfaces and the blank glass surface. The result can be understood by the increased substrate–cell interactions by coating of the HNTs. It can also be seen that the cells are uniformly distributed on the coatings without the formation of aggregates. The cells on the patterned HNTs coating indeed show a much more flat state (relatively large single cell area) compared with the cells on the control group. In order to further show the material–cell interface, the captured tumor cells were observed by SEM. From SEM photos of Fig. 5(B), the cell number on the patterned HNTs coating surface is significantly more than that on the blank glass substrates. The observed cell morphology is further investigated using a fluorescence microscope *via* staining the cell with DAPI and rhodamine phalloidin (Fig. 5(C)). The spreading areas of the cells increase gradually with the incubation time, and the cells on the patterned HNTs coating are flat as evidenced by the rich cytoskeleton. The cells captured by 2% (w/v) HNTs coating have more microfilaments in the microvilli and pseudopodia compared with those on the smooth surface and 1% (w/v) coating. The cytoskeletal intermediate filaments appear to impart tensile strength to the cell cytoplasm,[50] which leads to the fact that the cells turn from circular to irregular or polygonal in shape. The increased topographic interactions between nanotube coatings and tumor cells are facilitated for the application of HNTs in the capture of CTCs.

Fig. 5(D) shows the cell fluorescence microscopy images of the boundary of a smooth glass surface and a patterned HNTs coating. It is clear that the patterned HNTs coating can capture more much tumor cells, suggesting the increased cell–substrate interactions due to the rough surface structure of the patterned HNTs coating. Moreover, the microstructure of the cells on the smooth and rough surface is different from each other (Fig. 5(E)). Cells with fully extended pseudopodia attached to the patterned HNTs surface formed by self-assembly of nanotubes can clearly be observed. However, the MCF-7 cells on the smooth glass surface are rare and exhibit a rounded conformation with few extended pseudopodia. The nanorough surface can stimulate the cells to secrete more extracellular matrix (ECM),[51] which makes cells attach well on the surface of substrates. The MCF-7 cell outgrew long protrusions which connects the nanotubes. It can be inferred that the tumor cells are more likely to grasp the rough HNTs coating surface rather than the smooth glass surface, which may result from more van der Waals forces created by nanotube surfaces than the flat surface. The AFM result also confirmed the enhanced interactions between HNTs coatings and tumor cells (Fig. S3, ESI†). The improved cell–nanotube interface is attributed to the synergistic topographic interactions that occurred between the nanostructure-induced matching effect and the microstructure induced nano-synapses trap effect.[10]

A large amount of research proves that the capture yield of tumor cells by nanosurfaces can be further increased by conjugating antibody (such as anti-EpCAM[52]) or protein.[53] The patterned HNTs coating was conjugated with a cancer cell targeting antibody anti-EpCAM (Fig. S4, ESI†). The cells captured were evidenced by a DAPI-staining fluorescence image and the number was counted *via* the ImageJ software to quantify their cell capture efficiency (Fig. 6(A) and (B)). It can be seen that the anti-EpCAM conjugated smooth glass surface can capture more tumor cells than the raw smooth glass surface, and the HNTs coating conjugated with anti-EpCAM also shows much higher capture yield than that of the same HNTs coating without the conjugation of antibody. As can be seen from the statistical graph (Fig. 6(B)), after 2 h of incubation, the cell capture efficiency of the HNTs coating conjugated with anti-EpCAM is close to 80%, which is more than 3 and 4.5 times compared to the unmodified HNTs coating and the blank glass surface respectively. After 3 h of incubation, the capture yield of MCF-7 cells by the anti-EpCAM conjugated HNTs coating reaches up to 92% which is much higher than that of the unmodified HNTs coating (79.4%) and the smooth glass surface conjugated with anti-EpCAM (34.3%), which shows the topology formed by HNTs is more beneficial to the adhesion of tumor cells. The capture yield of MCF-7 cells by HNTs is comparable with the previously prepared anti-EpCAM conjugated reduced GO film (92% $\pm$ 4%).[6] The maximum tumor cell capture yield of the anti-EpCAM conjugated polystyrene nanotube surfaces is only 80%.[16] A high capture yield of 95% of MCF-7 cells can be achieved on the bovine serum albumin (BSA)-aptamer modified TiO_2 nanorod array substrates.[4] Although the micro- and nano-roughness on the glass surface can be obtained just by micro-scratching, it is hard to tailor the roughness level. Nanorough glass surfaces generated by reactive ion etching technology also show high capture yield of tumor cells (maximum capture yield of 95.4% for MD-MB-231 cells);[54] however, the reactive ion etching method needs large equipment and complicated controlling conditions.

The patterned HNTs coating was further used to capture the tumor cells spiked in peripheral blood samples. The artificial whole blood samples were prepared by spiking healthy human blood with MCF-7 cells at concentrations of approximately 10, 20, 50, 100, and 200 cells mL^{-1}. The anti-EpCAM conjugated patterned HNTs coatings provide 73–82% capture efficiency of targeted MCF-7 cells (Fig. 6(C)). For example, 8 spiked cells can be captured on the HNTs coating when we spiked 10 MCF-7 cells into the blood. In contrast, more than 82% spiked MCF-7

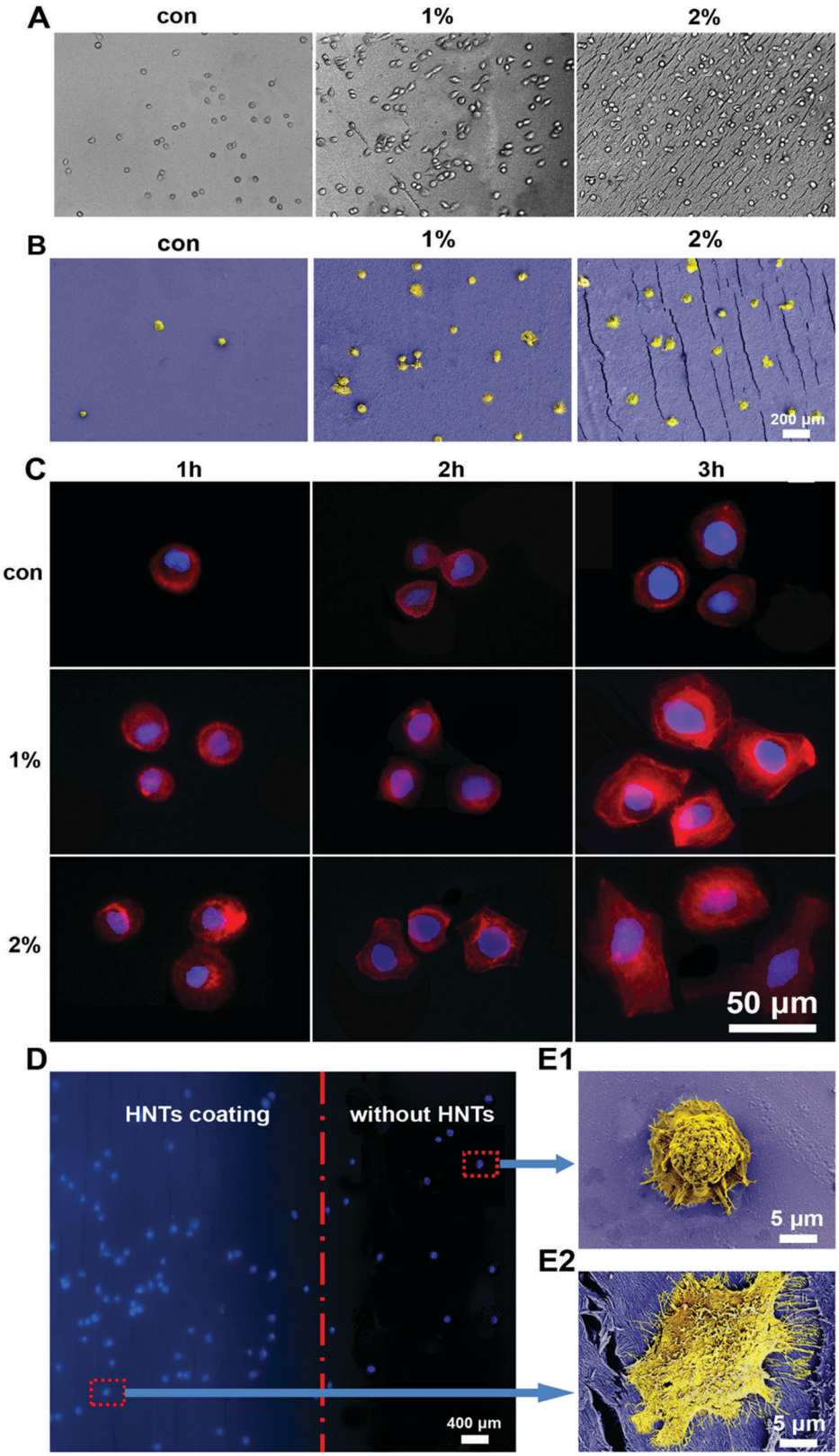

Fig. 5 The optical images of captured cells of MCF-7 on a blank glass surface and 1% (w/v) PSS-HNTs coating, and 2% (w/v) PSS-HNTs coating (A); SEM image of the MCF-7 cell captured on the blank glass surface, the 1% (w/v) HNTs coating and 2% (w/v) HNTs coating (B); the rhodamine phalloidin and DAPI fluorescence microscopy images of captured cells of MCF-7 on the smooth glass, 1% (w/v) PSS-HNTs coating, 2% (w/v) PSS-HNTs coating for 1, 2, and 3 hours (C). DAPI stained image micrograph of the MCF-7 cells captured on the patterned HNTs coating and blank glass substrate (D); SEM images of the microstructure topography of the cell on smooth blank glass (E1) and HNTs coatings (E2).

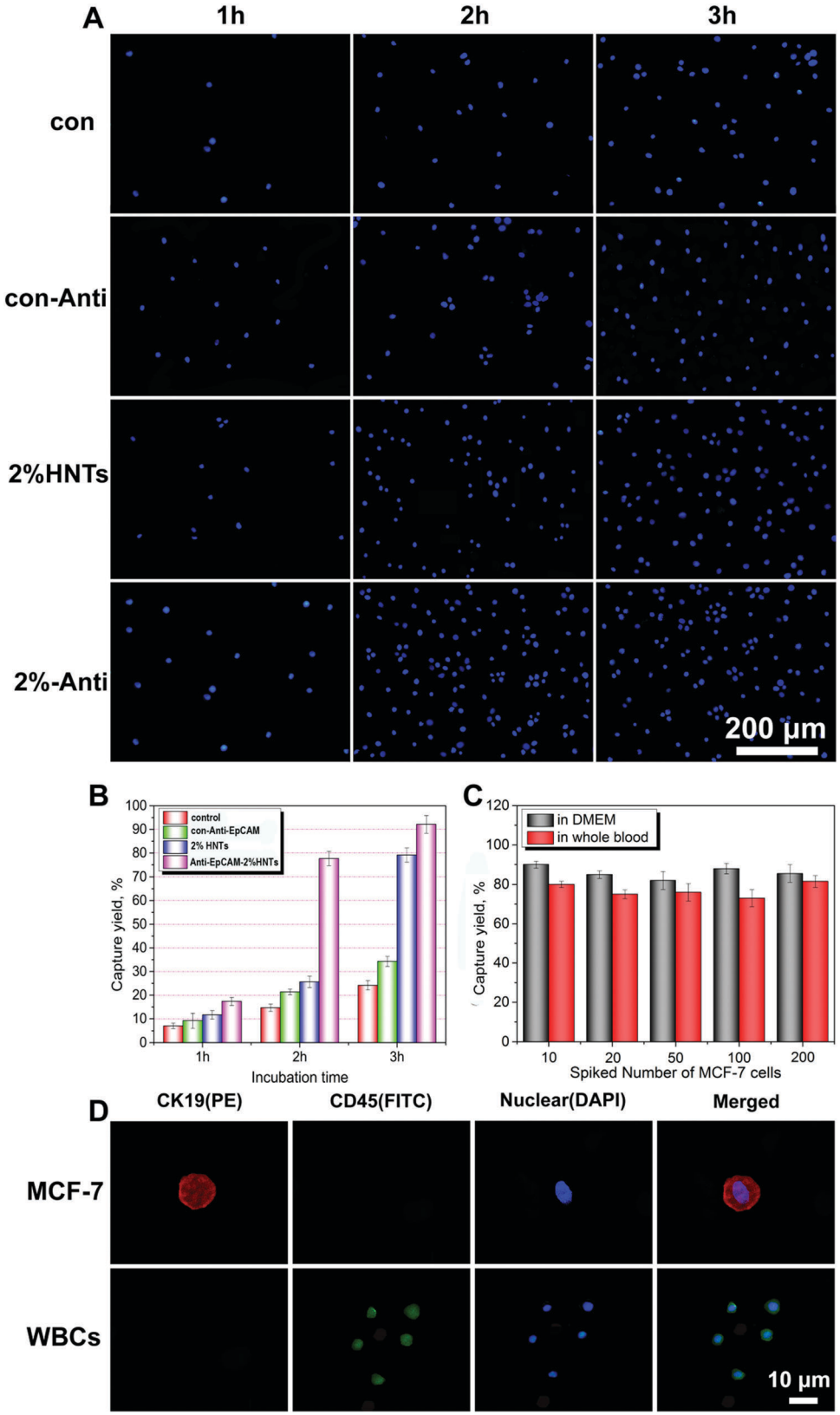

Fig. 6 DAPI stained fluorescence microscopy images of captured MCF-7 cells on the smooth glass and 2% (w/v) HNTs coating conjugated without and with anti-EpCAM (A); MCF-7 cells capture yield on different surfaces with different incubation times (B); the capture efficiency of MCF-7 cells on anti-EpCAM-coated HNTs coatings for DMEM and artificial whole blood samples with concentrations of 10, 20, 50, 100, and 200 cells mL^{-1} (n = 3) (C); three-color immunocytochemistry method for identifying spiked MCF-7 cells from white blood cells (WBCs) including PE-labeled anti-CK19 (CK19, a proteinmarker for epithelial cells), FITC-labeled anti-CD45 (CD45, a marker for WBCs) and DAPI for nuclear staining (D).

can be captured by the antibody conjugated HNTs coating from DEME. The difference in capture efficiency derives from the difference of liquid viscosity (the blood has a relatively high viscosity compared with the DEME), as the high viscosity leads to the less contact opportunity for the HNTs coating and the targeted cells. The capture efficiency of the HNTs coating towards MCF-7 cells is comparable with that of the TiO_2 nanorod arrays.[4] Fig. 6(D) shows the fluorescence images of the captured cells by the HNTs coating from the artificial whole blood samples. The tumor cells exhibit strong CK19 expression (red color) and WBCs present strong CD45 expression (green color). The tumor cells are larger than the WBCs (also shown in Fig. S5, ESI†). The size of WBCs is generally less than 15 μm.[55] The capture purity of cancer cells from spiked blood samples was also calculated. For example, more than 80% of the added tumor cells were captured by HNTs coating from the spiked blood with 100 MCF-7 cells after 3 h; meanwhile about 1000 white blood cells were captured. The number of white blood cells is 4×10^6–1×10^7 in a 1 mL healthy human blood sample. The calculated captured yield of white blood cells is 0.01–0.025%. Therefore, the capture purity of tumor cells from the spiked blood samples is more than 8%. After the combination of the images (Fig. 6D), the tumor cells (CK19+/CD45−/DAPI+) can be easily identified from WBCs (CK19−/CD45+/DAPI+). In total, the patterned HNTs coating prepared *via* self-assembly in a confined space shows promising application in clinical CTC capture for early diagnosis and monitoring of cancer patients.

4. Conclusions

A patterned HNTs coating on a glass substrate was prepared *via* nanotube self-assembly in a slit-like confined space. The dispersion and stability of HNTs in water are increased by PSS modification. HNTs can form stripe-like coating *via* the evaporation induced self-assembly process. The formed strips are more regular and almost parallel to each other when the HNTs concentration increases. The patterned HNTs coating formed from 2% PSS-HNTs dispersion has the maximum nanotube alignment degree. The surface roughness of the patterned HNTs coatings increases with the HNTs dispersion concentration. The patterned HNTs surfaces show high capture yield for the tumor cells and show relatively low capture yield for normal cells. The captured tumor cell numbers on HNTs rough surfaces are much greater and the cells exhibit much flatter morphology compared with those on the smooth glass surfaces. The captured cells form large protrusions on the rough HNTs surface and HNTs can stimulate cells to produce a large amount of ECM and crisscross cell filaments. The anti-EpCAM conjugated HNTs coating shows a maximum of 92% capture yield towards MCF-7 cells. The patterned HNTs coating can also capture rare tumor cells from peripheral blood samples. In total, the patterned HNTs coatings prepared from evaporation induced self-assembly show promising application in clinical CTC capture for early diagnosis and monitoring of cancer patients.

Acknowledgements

This work was financially supported by the National High Technology Research and Development Program of China (2015AA020915), the National Natural Science Foundation of China (grant no. 51473069 and 51502113), and the Guangdong Natural Science Funds for Distinguished Young Scholars (grant no. S2013050014606), the Science and Technology Planning Project of Guangdong Province (2014A020217006), the Guangdong Special Support Program (2014TQ01C127), the Special Fund for Ocean-Scientific Research in the public interest (201405105), and the Pearl River S&T Nova Program of Guangzhou (201610010026).

References

1 X. Yao, R. Peng and J. Ding, *Adv. Mater.*, 2013, **25**, 5257–5286.
2 R. He, L. Zhao, Y. Liu, N. Zhang, B. Cheng, Z. He, B. Cai, S. Li, W. Liu, S. Guo, Y. Chen, B. Xiong and X.-Z. Zhao, *Biomed. Microdevices*, 2013, **15**, 617–626.
3 M. J. Mitchell, C. A. Castellanos and M. R. King, *Biomaterials*, 2015, **56**, 179–186.
4 N. Sun, X. Li, Z. Wang, R. Zhang, J. Wang, K. Wang and R. Pei, *ACS Appl. Mater. Interfaces*, 2016, **8**, 12638–12643.
5 N. Zhang, Y. Deng, Q. Tai, B. Cheng, L. Zhao, Q. Shen, R. He, L. Hong, W. Liu and S. Guo, *Adv. Mater.*, 2012, **24**, 2756–2760.
6 Y. Li, Q. Lu, H. Liu, J. Wang, P. Zhang, H. Liang, L. Jiang and S. Wang, *Adv. Mater.*, 2015, **27**, 6848–6854.
7 H. J. Yoon, T. H. Kim, Z. Zhang, E. Azizi, T. M. Pham, C. Paoletti, J. Lin, N. Ramnath, M. S. Wicha, D. F. Hayes, D. M. Simeone and S. Nagrath, *Nat. Nanotechnol.*, 2013, **8**, 735–741.
8 P. Kocbek, N. Obermajer, M. Cegnar, J. Kos and J. Kristl, *J. Controlled Release*, 2007, **120**, 18–26.
9 W. Chen, S. Weng, F. Zhang, S. Allen, X. Li, L. Bao, R. H. Lam, J. A. Macoska, S. D. Merajver and J. Fu, *ACS Nano*, 2012, **7**, 566–575.
10 S. Wang, H. Wang, J. Jiao, K. J. Chen, G. E. Owens, K. i. Kamei, J. Sun, D. J. Sherman, C. P. Behrenbruch and H. Wu, *Angew. Chem.*, 2009, **121**, 9132–9135.
11 S. T. Kim, D.-J. Kim, T.-J. Kim, D.-W. Seo, T.-H. Kim, S.-Y. Lee, K. Kim, K.-M. Lee and S.-K. Lee, *Nano Lett.*, 2010, **10**, 2877–2883.
12 B. Wang, A. L. Weldon, P. Kumnorkaew, B. Xu, J. F. Gilchrist and X. Cheng, *Langmuir*, 2011, **27**, 11229–11237.
13 S. Hou, H. Zhao, L. Zhao, Q. Shen, K. S. Wei, D. Y. Suh, A. Nakao, M. A. Garcia, M. Song and T. Lee, *Adv. Mater.*, 2013, **25**, 1547–1551.
14 J. Sekine, S. C. Luo, S. Wang, B. Zhu, H. R. Tseng and H. h. Yu, *Adv. Mater.*, 2011, **23**, 4788–4792.
15 H. Liu, X. Liu, J. Meng, P. Zhang, G. Yang, B. Su, K. Sun, L. Chen, D. Han and S. Wang, *Adv. Mater.*, 2013, **25**, 922–927.
16 X. Liu, L. Chen, H. Liu, G. Yang, P. Zhang, D. Han, S. Wang and L. Jiang, *NPG Asia Mater.*, 2013, **5**, e63.

17 X. Hu and S. Liu, *Dalton Trans.*, 2015, **44**, 3904–3922.
18 R. Qi, R. Guo, M. Shen, X. Cao, L. Zhang, J. Xu, J. Yu and X. Shi, *J. Mater. Chem.*, 2010, **20**, 10622–10629.
19 Y. Lvov and E. Abdullayev, *Prog. Polym. Sci.*, 2013, **38**, 1690–1719.
20 M. Liu, Z. Jia, D. Jia and C. Zhou, *Prog. Polym. Sci.*, 2014, **39**, 1498–1525.
21 G. I. Fakhrullina, F. S. Akhatova, Y. M. Lvov and R. F. Fakhrullin, *Environ. Sci.: Nano*, 2015, **2**, 54–59.
22 Y. Lvov, W. Wang, L. Zhang and R. Fakhrullin, *Adv. Mater.*, 2016, **28**, 1227–1250.
23 X. Hu, G. Liu, Y. Li, X. Wang and S. Liu, *J. Am. Chem. Soc.*, 2014, **137**, 362–368.
24 M. Liu, Y. Chang, J. Yang, Y. You, R. He, T. Chen and C. Zhou, *J. Mater. Chem. B*, 2016, **4**, 2253–2263.
25 M. Liu, C. Wu, Y. Jiao, S. Xiong and C. Zhou, *J. Mater. Chem. B*, 2013, **1**, 2078–2089.
26 E. A. Naumenko, I. D. Guryanov, R. Yendluri, Y. M. Lvov and R. F. Fakhrullin, *Nanoscale*, 2016, **8**, 7257–7271.
27 R. Qi, R. Guo, F. Zheng, H. Liu, J. Yu and X. Shi, *Colloids Surf., B*, 2013, **110**, 148–155.
28 V. Vergaro, E. Abdullayev, Y. M. Lvov, A. Zeitoun, R. Cingolani, R. Rinaldi and S. Leporatti, *Biomacromolecules*, 2010, **11**, 820–826.
29 M. Kryuchkova, A. Danilushkina, Y. Lvov and R. Fakhrullin, *Environ. Sci.: Nano*, 2016, **3**, 442–452.
30 A. D. Hughes and M. R. King, *Langmuir*, 2010, **26**, 12155–12164.
31 M. J. Mitchell, C. A. Castellanos and M. R. King, *J. Biomed. Mater. Res., Part A*, 2015, **103**, 3407–3418.
32 A. D. Hughes, J. Mattison, J. D. Powderly, B. T. Greene and M. R. King, *J. Visualized Exp.*, 2012, e4248.
33 A. D. Hughes, J. Mattison, L. T. Western, J. D. Powderly, B. T. Greene and M. R. King, *Clin. Chem.*, 2012, **58**, 846–853.
34 M. J. Mitchell, C. S. Chen, V. Ponmudi, A. D. Hughes and M. R. King, *J. Controlled Release*, 2012, **160**, 609–617.
35 M. Liu, R. He, J. Yang, W. Zhao and C. Zhou, *ACS Appl. Mater. Interfaces*, 2016, **8**, 7709–7719.
36 Y. Zhao, G. Cavallaro and Y. Lvov, *J. Colloid Interface Sci.*, 2015, **440**, 68–77.
37 R. He, L. Zhao, Y. Liu, N. Zhang, B. Cheng, Z. He, B. Cai, S. Li, W. Liu and S. Guo, *Biomed. Microdevices*, 2013, **15**, 617–626.
38 G. Cavallaro, G. Lazzara and S. Milioto, *J. Phys. Chem. C*, 2012, **116**, 21932–21938.
39 D. Maji, S. Lahiri and S. Das, *Surf. Interface Anal.*, 2012, **44**, 62–69.
40 M. Abkarian, J. Nunes and H. A. Stone, *J. Am. Chem. Soc.*, 2004, **126**, 5978–5979.
41 W. Han and Z. Lin, *Angew. Chem., Int. Ed.*, 2012, **51**, 1534–1546.
42 L. R. Parent, D. B. Robinson, T. J. Woehl, W. D. Ristenpart, J. E. Evans, N. D. Browning and I. Arslan, *ACS Nano*, 2012, **6**, 3589–3596.
43 M. Byun, W. Han, B. Li, X. Xin and Z. Lin, *Angew. Chem., Int. Ed.*, 2013, **52**, 1122–1127.
44 Q. Zhou, J. Xie, M. Bao, H. Yuan, Z. Ye, X. Lou and Y. Zhang, *J. Mater. Chem. B*, 2015, **3**, 4439–4450.
45 M. Mahmoudi, S. Bonakdar, M. A. Shokrgozar, H. Aghaverdi, R. Hartmann, A. Pick, G. Witte and W. J. Parak, *ACS Nano*, 2013, **7**, 8379–8384.
46 H. Jeon, C. G. Simon and G. Kim, *J. Biomed. Mater. Res., Part B*, 2014, **102**, 1580–1594.
47 A. T. Nguyen, S. R. Sathe and E. K. Yim, *J. Phys.: Condens. Matter*, 2016, **28**, 183001.
48 A. Muller, B. Homey, H. Soto, N. Ge, D. Catron, M. E. Buchanan, T. McClanahan, E. Murphy, W. Yuan, S. N. Wagner, J. L. Barrera, A. Mohar, E. Verastegui and A. Zlotnik, *Nature*, 2001, **410**, 50–56.
49 I. Abrahamsson, T. Berglundh, E. Linder, N. P. Lang and J. Lindhe, *Clin. Oral Implants Res.*, 2004, **15**, 381–392.
50 R. D. Goldman, S. Khuon, Y. H. Chou, P. Opal and P. M. Steinert, *J. Cell Biol.*, 1996, **134**, 971–983.
51 B. Alberts, A. Johnson, J. Lewis, M. Raff, K. Roberts and P. Walter, *Molecular Biology of the Cell*, Garland Publishing, New York, 5th edn, 2007, ch. 19, pp. 1131–1204.
52 S. Nagrath, L. V. Sequist, S. Maheswaran, D. W. Bell, D. Irimia, L. Ulkus, M. R. Smith, E. L. Kwak, S. Digumarthy and A. Muzikansky, *Nature*, 2007, **450**, 1235–1239.
53 P. Vajkoczy, M. Laschinger and B. Engelhardt, *J. Clin. Invest.*, 2001, **108**, 557–565.
54 W. Q. Chen, S. N. Weng, F. Zhang, S. Allen, X. Li, L. W. Bao, R. H. W. Lam, J. A. Macoska, S. D. Merajver and J. P. Fu, *ACS Nano*, 2013, **7**, 566–575.
55 J. Meng, P. Zhang, F. Zhang, H. Liu, J. Fan, X. Liu, G. Yang, L. Jiang and S. Wang, *ACS Nano*, 2015, **9**, 9284–9291.